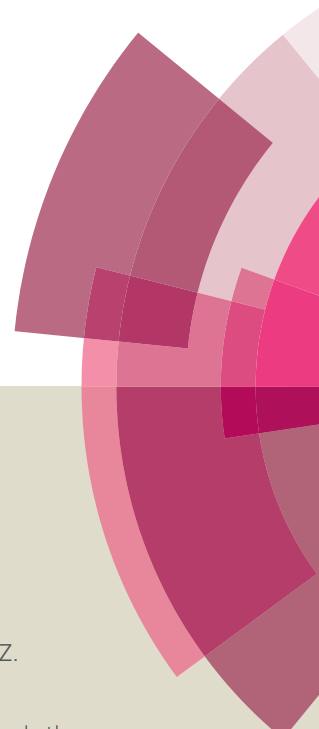


Catalysis Science & Technology

Accepted Manuscript



This article can be cited before page numbers have been issued, to do this please use: F. W. Fu, Y. Xu, Z. Fu, S. Cao and Y. Chen, *Catal. Sci. Technol.*, 2016, DOI: 10.1039/C6CY01568A.



This is an *Accepted Manuscript*, which has been through the Royal Society of Chemistry peer review process and has been accepted for publication.

Accepted Manuscripts are published online shortly after acceptance, before technical editing, formatting and proof reading. Using this free service, authors can make their results available to the community, in citable form, before we publish the edited article. We will replace this *Accepted Manuscript* with the edited and formatted *Advance Article* as soon as it is available.

You can find more information about *Accepted Manuscripts* in the [Information for Authors](#).

Please note that technical editing may introduce minor changes to the text and/or graphics, which may alter content. The journal's standard [Terms & Conditions](#) and the [Ethical guidelines](#) still apply. In no event shall the Royal Society of Chemistry be held responsible for any errors or omissions in this *Accepted Manuscript* or any consequences arising from the use of any information it contains.

ARTICLE

Highly selective oxidation of sulfides on a CdS/C₃N₄ catalyst with dioxygen under visible-light irradiation†

Cite this: DOI: 10.1039/x0xx00000x

Yong Xu,^a Zi-Cheng Fu,^a Shuang Cao,^a Yong Chen^a and Wen-Fu Fu^{*ab}

A CdS/C₃N₄ composite photocatalyst was fabricated by a facile method, and its structure, composition, and morphology were characterized in detail. The catalyst exhibited highly photocatalytic products selectivity towards the oxidation of sulfides into corresponding sulfoxides even when the irradiation time was extended to 20 h. The synergistic effect between CdS and C₃N₄ gave rise to efficient interfacial transfer of photogenerated electrons and holes on both materials, as confirmed by transient photocurrent measurements. The best photocatalytic activity for the catalyst prepared at 300 °C was achieved at a C₃N₄/CdS ratio of 0.3. Sulfides were efficiently oxidized to sulfoxides with dioxygen under visible-light illumination in methanol at room temperature. The conversion efficiency of sulfides with electron-withdrawing groups was lower than that of those with a donating substituent, and the conversion strongly depended on the steric hindrance effect of the substituent. A possible photocatalytic mechanism was proposed based on electron spin resonance, trapping experiments, and other experimental results.

Received 00th January 2012,
Accepted 00th January 2012

DOI: 10.1039/x0xx00000x

www.rsc.org/

1. Introduction

Photocatalytic reactions have received growing interest owing to the worsening energy crisis and urgent environmental problems.^{1–3} The copious amount of solar energy available as a clean and economical energy source has promoted the exploration of new methods to convert solar energy to chemical energy.^{4–5} Sulfoxides have played an important role as intermediates in the synthesis of pharmaceuticals, agrochemicals, and other fine chemicals.^{6–8} Generally, the most common way to prepare sulfoxides is the oxidation of the corresponding sulfides. Traditionally, oxidants with high oxidative capacity have been used for this purpose, such as trifluoroacetic acid,⁸ Zn(MnO₄)₂,⁹ nitric acid,¹⁰ meta-chloroperoxybenzoic acid,¹¹ and metallic oxides.^{12–14} However, these oxidants have low product selectivity because of uncontrollable over-oxidation to sulfones. Moreover, a great excess of oxidant is used and accompanied by the generation of toxic byproducts. In the last few decades, hydrogen peroxide with catalytic amounts of catalysts such as metal complexes,^{15,16} metal-salts,^{17,18} inorganic-organic hybrids,¹⁹ and enzymes²⁰ has also been studied as an oxidant. Nonetheless, compared with photocatalysis, these thermal catalytic systems are power wasting and environmentally hazardous, especially in industrial application.

Recently, a ruthenium-based dyad system constituting a photosensitizer and a catalyst, namely Ru_{phot}-Ru_{cat}-OH₂, has been proved to selectively catalyze sulfide oxygenation.^{21,22} Our group previously reported the photocatalytic oxidation of sulfide into the corresponding sulfoxide in neutral aqueous solution using ruthenium(II) chromophore-catalyst dyad

catalyst, and demonstrated the occurrence of oxygen atom transfer from water to the substrate through isotopic labeling experiments.²³ Sun and co-workers developed a robust system with an inorganic semiconductor material as photosensitizer and a Ru-aqua complex as a catalyst to drive sulfide oxidation.²⁴ Additionally, an iron(IV)-oxo species has been used to oxidize the radical sulfide cations to the corresponding sulfoxide through in-situ-generated [Ru^{III}(bpy)₃]³⁺.²⁵ Nevertheless, these photocatalytic systems require a large excess of sacrificial electron acceptors such as [Co(NH₃)₅Cl]Cl₂ and Na₂S₂O₈. From the viewpoint of green and sustainable chemistry, molecular oxygen, an ideal oxidant, is omnipresent and thus readily available for the oxidation of sulfides.²⁶ However, the fact that the triplet ground state of oxygen is an inactive species and singlet-state oxygen is highly reactive once activated is a challenge. Chen and co-workers employed TiO₂ as a photocatalyst to achieve the aerobic oxidation of sulfide and the aerobic oxidative formylation of amine with methanol in the same system.²⁷ Subsequently, they used triethylamine as a redox mediator to realize the aerobic oxidation of sulfides into sulfoxides under visible-light irradiation.²⁸ A system including mesoporous graphite-like carbon nitride (mpg-C₃N₄) and isobutyraldehyde with highly visible-light catalytic activity towards the selective oxidation of sulfide to sulfoxide was reported by Zhang et al.²⁹ This material has recently been used as a photocatalyst for the transformation of organic substrates.^{30–33} Li and co-workers also reported the successful photocatalytic oxidation of sulfides on Pt/BiVO₄ in water under visible-light illumination; however, the conversion efficiency was poor.³⁴

CdS is one of the most attractive photocatalysts owing to its highly efficient visible-light absorption.³⁵ However, it also

suffers from several defects such as photocorrosion that impede its wide application.^{36–38} Considering the relatively well-matching band edges of CdS and C₃N₄, it is possible that corrosive photogenerated holes from the valence band of CdS can readily transfer to C₃N₄ and thereby facilitate electron-hole pairs separation.³⁹ Therefore, coupling CdS with C₃N₄ is expected to be a simple method of enhancing the conversion efficiency and product selectivity of the oxidation of sulfides to corresponding sulfoxides.

Herein, we report a facile method of preparing an organic-inorganic heterogeneous CdS/C₃N₄ (cdcn) photocatalyst with closely contacting interfaces. C₃N₄ can easily be exfoliated into thin sheets by ultrasonication, thereby providing many binding sites for anchoring CdS nanoparticles. This strategy reduces the aggregation of CdS and improves the stability of the photocatalyst. The resulting composite catalyst showed significantly enhanced photocatalytic activity and product selectivity for the oxidation of sulfides under visible-light irradiation. Furthermore, the electronic and steric hindrance effects of substituents on the sulfides were found to have an intense effect on the photocatalytic sulfide to sulfoxide conversion efficiency.

2. Experimental

2.1 Preparation

All reagents were purchased from commercial sources and used as received without further purification. The C₃N₄ powder⁴⁰ was obtained by directly heating urea (10 g) in a muffle furnace at 550 °C for 4 h at a heating rate of 0.5 °C min⁻¹. After the furnace was cooled to room temperature, the resulting faint yellow product was collected and milled into powder for further use.

2.1.1 Preparation of CdS nanoparticles

CdS nanoparticles were fabricated according to a modified literature method.⁴¹ In a typical procedure, 400 mL (0.14 M) of aqueous Na₂S solution was added slowly to 500 mL (0.14 M) of Cd(OAc)₂ solution with vigorous stirring. The resulting yellow precipitate was stirred for 24 h and then allowed to settle for 48 h. The yellow slurry was filtered and washed with 200 mL of water, then transferred to a dried Teflon-lined autoclave with a capacity of 100 mL. The autoclave was sealed and heated at 200 °C for 72 h, after which the system was allowed to cool to room temperature naturally. The obtained yellow solid was filtered and then washed with 500 mL of water and 100 mL of ethanol consecutively. After drying at 80 °C for 5 h in the oven, the obtained yellow solid was ground into fine particles and used in the following step.

2.1.2 Preparation of CdS/C₃N₄ composite photocatalyst

The CdS/C₃N₄ hybrid photocatalyst was prepared as follows. The as-prepared C₃N₄ was dispersed in 80 mL deionized water and stirred for 30 min. The suspension was then transferred to an ultrasonic environment for another 60 min to exfoliate it into sheets. After that, 100 mg of the CdS powder was added to the above solution and stirred for a further 30 min. The mixture was then ultrasonicated for 2 h to completely disperse it. Subsequently, the powder was collected by filtration, washed with distilled water several times, and dried at 70 °C overnight. Finally, the sample was heated at 300 °C for 4 h in a muffle furnace. A series of CdS/C₃N₄ composites containing a fixed amount of CdS (100 mg) and a varied mass of C₃N₄ (10, 20, 30,

40, and 50 mg) were prepared. The samples were marked as cdcn(χ), where χ is the mass of C₃N₄. The catalysts used in the present study were prepared at 300 °C unless otherwise noted. A similar procedure was used to prepare CdS/C₃N₄ photocatalysts at 200, 250, 350, and 400 °C.

2.2 Characterization

The samples were characterized by powder X-ray diffraction (XRD) on a Bruker AXS D8 X-ray diffractometer with Cu K α (λ = 1.54056 Å) to identify their phases. Scanning electron microscopy (SEM) and energy dispersive X-ray (EDX) spectroscopy measurements were conducted on a Hitachi S-4800 field emission scanning electron microscope. The particle size and lattice fringes of the samples were analyzed on a transmission electron microscope (TEM; JEM 2100F) with an accelerating voltage of 200 kV. Fourier transform infrared spectroscopy (FTIR) data was collected using the standard KBr disk method at ambient temperature on a Bruker ALPHA FTIR spectrometer from 4000 to 400 cm⁻¹. Ultraviolet-visible diffuse reflectance spectra (DRS) was recorded on a spectrophotometer (Hitachi UV-3010) using BaSO₄ as a reference. Photoluminescence spectra (PL) was measured at room temperature under excitation at 325 nm (Hitachi F-4500). X-ray photoelectron spectroscopy (XPS) was carried out on a PHI 5300 ESCA using an Al K α X-ray source with a power of 250 W. The charge effect was calibrated using the binding energy of C1s. Thermogravimetric analysis was performed on a TA Instrument Q600 SDT from room temperature to 800 °C. Electron spin resonance (ESR) signals were recorded at room temperature with a Bruker ESR E500 spectrometer.

2.3 Typical procedure for catalytic oxidation of methyl p-methoxyphenyl sulfide and other sulfides

Typically, 3 mL of a solution containing 1 mmol substrate and 5 mg CdS/C₃N₄ photocatalyst was added to a 15-mL cuvette sealed with a rubber septum placed on top of a magnetic stirrer. A stream of dioxygen was then passed into the reaction system for 10 min and filled again every 2 h. White light-emitting diodes (LEDs) (30 × 3 W, λ ≥ 420 nm) were used as the irradiation light source. The LEDs were positioned 3 cm away from the sample, which was kept under continuous stirring at room temperature. The mixture was stirred for 30 min before irradiation. After the reaction, dimethyl p-benzenedicarboxylate was added to the mixture as an internal standard. The chemical structure and the quantity of the products were determined by ¹H nuclear magnetic resonance (NMR) spectroscopy (BrukerAvance 400 spectrometer). The conversion of sulfide and the selectivity for sulfoxide were calculated from the equations:

$$\text{conversion (\%)} = \frac{n_{\text{consumed sulfide}}}{n_{\text{initial sulfide}}} \times 100$$

$$\text{selectivity (\%)} = \frac{n_{\text{sulfoxide}}}{n_{\text{consumed sulfide}}} \times 100$$

Cycling tests: 3 mL of methanol containing 1 mmol methyl p-methoxyphenyl sulfide and 5 mg cdcn(30) was added into a 15-mL cuvette sealed with a rubber septum. After the sample filled with dioxygen was irradiated for 5 h, the obtained mixture was centrifuged and washed 3 times with methanol. The two parts of liquid was merged, the chemical structure and the quantity of the products were determined by NMR analysis. The remaining solid was dried in vacuum oven to use as the next time. Same process was conducted for next 3 times.

2.4 Photoelectrochemical (PEC) measurements

Photocurrent measurements were conducted on a CHI 660C electrochemical workstation (Chenhua Instrument, China) using a conventional three-electrode configuration. A catalyst electrode served as the working electrode, with a platinum foil as the counter electrode and an Ag/AgCl (saturated KCl) electrode as the reference electrode. Then, 0.2 M of Na₂SO₄ aqueous solution (pH = 6.8) was used as the electrolyte, through which nitrogen was bubbled for 20 min prior to measurement. The white LED light source was used for irradiation. The working electrodes were prepared as follows: 2 mg of the as-prepared catalyst sample was dispersed in 30 μL N,N-dimethyl formamide by sonication for 20 min. The slurry was then evenly spread onto a 3.0 × 1.0 cm² conducting indium tin oxide glass substrate with an active area of about 1.0 cm². The film was dried in air and annealed at 150 °C for 1 h in flowing Ar atmosphere. The photoresponses of the samples at light on and off were measured at 0.0 V. Electrochemical impedance spectroscopy (EIS) measurements were carried out using an AC amplitude of 10 mV in the frequency range of 0.01 Hz–1000 kHz at 0.05 V.

3. Results and discussion

3.1 Characterization of photocatalysts

The XRD patterns of the as-prepared pure C₃N₄, pure CdS, and CdS/C₃N₄ composite synthesized with 30 mg C₃N₄ (mass ratio of C₃N₄/CdS, 30/100; marked as cdcn(30)) are shown in Fig. 1a. Two distinct diffraction peaks were found at 13.1° and 27.4° for the pure C₃N₄ sample (JCPDS Card No. 87-1526), corresponding to the interplanar separation and interlayer stacking of the conjugated aromatic segments, respectively, and indexed as the (100) and (002) planes.⁴² After ultrasonic exfoliation, the peak at 27.4° was much weaker (Fig. S1); this decreased intensity indicated that the interlayer structure was destroyed. The pure CdS sample was identified as hexagonal wurtzite CdS (JCPDS Card No. 65-3414). The two peaks of C₃N₄ nearly disappeared from the pattern of the cdcn(30) sample, suggesting that CdS nanoparticles without the surfactant as-prepared, with size ranging from 30 nm to 50 nm, either loaded on the surface of C₃N₄ sheets or embedded into the layers of C₃N₄. The SEM (Fig. 1b, c) and TEM (Fig. 1d, e) images intuitively showed that exfoliated C₃N₄ were decorated with CdS nanoparticles. Additionally, oxygen-containing defects and amino groups on the surface of the C₃N₄ likely served as anchoring sites to immobilize the CdS nanoparticles, which reduced their aggregation. The lattice spacing of 0.337 nm was ascribed to the (002) plane of CdS, the peak of which (26.5°) was very close and overlapped with that of C₃N₄ (27.4°). EDX analysis (Fig. S2) carried out on randomly selected areas revealed an approximate S:Cd ratio of 1:1 based on the calculated peak areas, confirming the successful formation of the desired phase. The peak of Si was attributed to the silicon pellet. EDX mapping further revealed that all elements were uniformly distributed in the cdcn (Fig. 1f–i).

XPS was employed to confirm the formation of the CdS/C₃N₄ heterogeneous catalyst and study its surface chemical state. The XPS

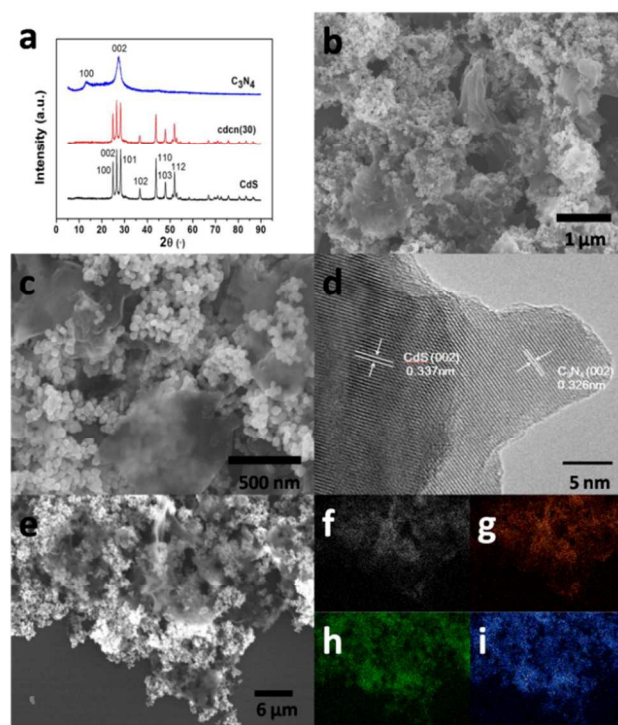


Fig. 1 (a) Powder XRD pattern and (b), (c) SEM images of cdcn(30), (d) HRTEM image of cdcn(30), (e) TEM image of cdcn(30), and corresponding EDX mappings (f, C-K; g, N-K; h, S-K; i, Cd-L).

spectrum (Fig. S3) of cdcn(30) showed that C, N, S, Cd, and a small amount of O elements existed in the sample. Fig. 2a–d show the high-resolution XPS spectra of C 1s, N 1s, S 2p, and Cd 3d. The C 1s spectrum could be separated into three peaks, at 284.4, 285.6, and 288.1 eV. The former peak was ascribed to graphitic *sp*² C-C bonds, while the last was identified as *sp*² hybridized C atoms on the N-containing aromatic rings (N=C=N), which represent the major carbon species in C₃N₄. The weak middle peak (285.6 eV) was assigned to *sp*³-bonded carbon from defects on the C₃N₄ surface.^{43,44} Peaks at 398.2, 399.7, and 401 eV were identified in the N 1s spectrum (Fig. 2b). The peak located at 398.2 eV was assigned to the *sp*²-bonded N in the triazine units (C-N=C)₄, while the weak peaks at 399.7 and 401 eV originated from central N in the triazine aromatic cycles and amino groups with a hydrogen atom (C-N-H), respectively.^{39,45} Comparison of the XPS spectrum of C₃N₄ with that of CdS/C₃N₄ revealed that the C 1s peak (285.6 eV) was shifted to higher binding energy, while the peaks at 398.2 eV and 401 eV for N 1s were shifted to lower binding energy. These shifts indicated electronic interaction between C₃N₄ and CdS, which is consistent with the FTIR (Fig. S4) results. Additionally, the XPS spectrum of S 2p (Fig. 2c) showed two peaks, at 161.3 eV (S 2p_{3/2}) and 162.4 eV (S 2p_{1/2}), which were ascribed to S²⁻ in CdS. The Cd 3d peaks (Fig. 2d) were observed at 404.9 eV and 411.7 eV, attributed to Cd 3d_{5/2} and Cd 3d_{3/2} for Cd²⁺ in CdS.⁴⁶ Moreover, the binding energies of S 2P (161.2 eV) and Cd 3d (411.6 eV) in cdcn(30) were slightly lower than those of the pure materials, which also suggests an interaction between CdS and C₃N₄.

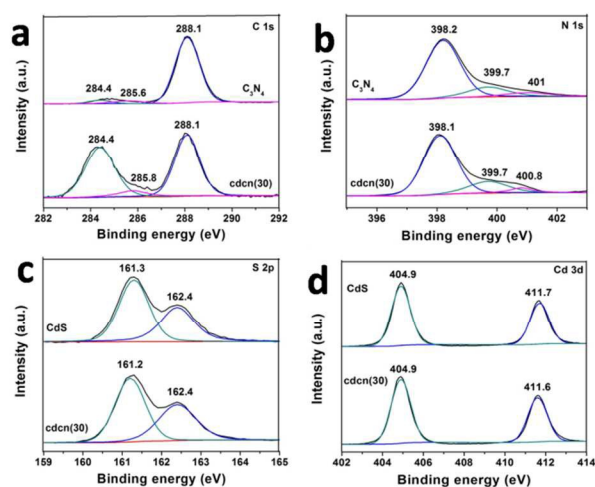


Fig. 2 High-resolution XPS spectra of (a) C 1s, (b) N 1s, (c) S 2p, and (d) Cd 3d in the samples.

Figure 3a depicts the typical ultraviolet-visible DRS of C_3N_4 , CdS, and cdcn. A clear redshift occurred from C_3N_4 to cdcn(30), which is favorable for the use of visible light. The band gaps of the samples were determined using the Tauc/David-Mott model described by the equation:⁴⁷ $(\alpha h\nu)^{1/n} = A(h\nu - E_g)$. The value of the exponent n denotes the nature of the sample transition and is defined as 0.5 for a directly allowed transition. The fitting results showed in Fig. 3b indicate that the band gap of pure C_3N_4 , CdS, and cdcn(30) was approximately 2.87 eV, 2.301 eV, and 2.327 eV, respectively. Because of the relatively high optical absorption coefficient of CdS in the visible region, the absorbance of cdcn(30) was slightly enhanced compared with that of C_3N_4 . Fig. 3c shows the transient photocurrent response of CdS and cdcn(30) during several on-off cycles. It was clear that the photocurrent response of cdcn(30) was significantly higher than that of CdS under the same visible-light illumination. The generated photocurrent was mainly the result of photoinduced electrons diffusing to the indium tin oxide.⁴⁸ Therefore, the enhanced photocurrent implied that a more effective charge transfer was achieved after the formation of the heterojunction. The strength of the photocurrent was in line with the order of photocatalytic activity. To further verify the above results, electrochemical impedance spectroscopy, a powerful tool used to analyze charge transfer properties and the efficiency of photogenerated charge carrier separation, was also performed.⁴⁹ As presented in Fig. 3d, the impedance radius of cdcn(30) was smaller than that of CdS and other cdcn samples. Generally, a smaller arc radius on EIS (Nyquist plots) represents a faster interfacial charge transfer and higher separation efficiency of photogenerated charge carriers. The results therefore demonstrated that cdcn(30) more favorably transferred and separated photogenerated charge carriers than the CdS particles. C_3N_4 displayed an intense photoluminescence, but the emissive intensity of cdcn(30) was remarkably weakened, indicating efficient transfer of photogenerated electrons and holes between CdS and C_3N_4 (Fig. S5).

3.2 Photocatalytic oxidation of sulfides

Photocatalysts (cdcn) with C_3N_4 to CdS mass ratios of 0.1–0.5 were also prepared, and the reaction temperature was varied

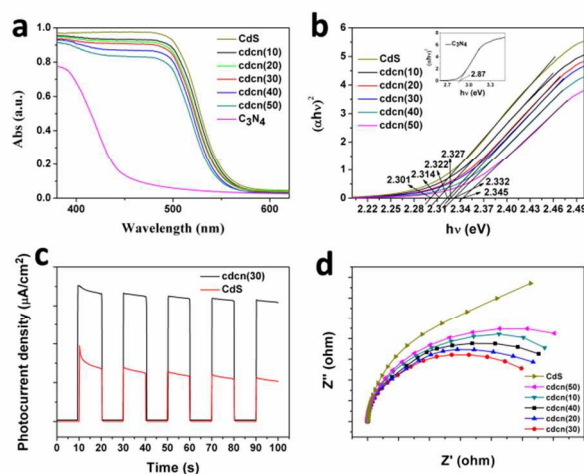


Fig. 3 (a) Ultraviolet-visible DRS of C_3N_4 , CdS, and cdcn, (b) corresponding plots of $(\alpha h\nu)^2$ versus energy ($h\nu$) for the band gap energy, (c) transient photocurrent response under visible light, and (d) EIS Nyquist plots of CdS and cdcn.

from 200 °C to 400 °C in 50 °C steps. To determine the optimal catalyst, the catalytic oxidation of methyl *p*-methoxyphenyl sulfide was performed using the as-prepared samples. Fig. 4a shows that the highest catalytic activity was obtained when the mass ratio of C_3N_4 to CdS was 0.3 and the preparation temperature was 300 °C. With increasing C_3N_4 content, the CdS nanoparticles would have been better dispersed and a larger number of active catalytic sites provided, but when the limiting value was reached, the adsorption of substrate molecules and light would have been restrained. The catalytic activity of the cdcn samples also exhibited a dependence on the catalyst preparation temperature. After thermal treatment, the interaction between CdS and C_3N_4 becomes stronger, which was proved by comparison of cdcn(30) and mechanical mixing of CdS and C_3N_4 . However, a significant decline in activity was observed when the preparation temperature was increased to 350 °C owing to the partial decomposition of CdS (inset in Fig. 4b). Thus, cdcn(30) prepared at 300 °C was selected as the photocatalyst for the following sulfide oxidation experiments. The surface areas of CdS and cdcn(30) are 32.039 m²/g and 47.356 m²/g respectively, which was estimated from the amount of N_2 adsorbed by using the BET equilibrium equation.

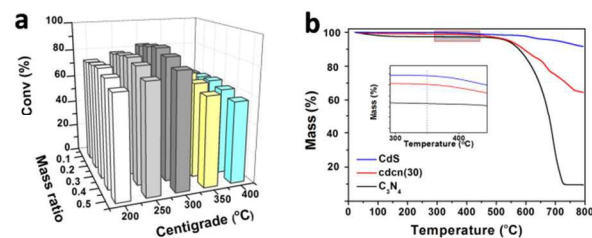
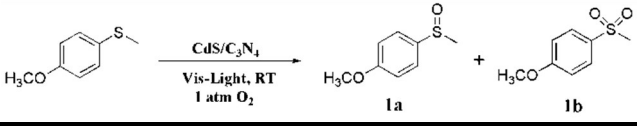


Fig. 4 (a) Photocatalytic activity of various cdcn samples prepared at different temperatures and different mass ratios of C_3N_4 to CdS. Methyl *p*-methoxyphenyl sulfide was used as the substrate, 3 mL CH_3OH was used as the solvent. (b) Thermogravimetric analysis results for CdS, C_3N_4 , and cdcn(30).

To optimize the reaction conditions for sulfide oxygenation, different solvents (Table 1, entry 1–6) were chosen with methyl *p*-methoxyphenyl sulfide as a model substrate. Methanol was found to be the preferable medium for this oxidation reaction

Table 1 Photocatalytic oxidation of methyl p-methoxyphenyl sulfide under various conditions


Entry	Catalyst	Solvent	Conv. (%)	Sel. (%)	
				1a	1b
1	cdcn(30)	CH ₃ OH	88.1	97	3
2	cdcn(30)	CH ₃ CN	17.0	100	0
3	cdcn(30)	CH ₂ Cl ₂	2.1	100	0
4	cdcn(30)	acetone	1.6	100	0
5	cdcn(30)	H ₂ O	7.1	100	0
6	cdcn(30)	THF	6.0	100	0
7	CdS	CH ₃ OH	61.0	97	3
8	C ₃ N ₄	CH ₃ OH	3.1	100	0
9 ^a	cdcn(30)	CH ₃ OH	0	—	—
10 ^b	CdS-C ₃ N ₄	CH ₃ OH	66.9	97	3
11 ^c	—	CH ₃ OH	0	—	—
12 ^d	cdcn(30)	CH ₃ OH	0	—	—
13 ^e	cdcn(30)	CH ₃ OH	44.6	97	3
14 ^f	cdcn(30)	CH ₃ OH	100	97	3
15 ^g	cdcn(30)	CH ₃ OH	52.6	100	0
16 ^h	cdcn(30)	CH ₃ OH	11.5	99	1

Reaction conditions: methyl p-methoxyphenyl sulfide 1 mmol, catalyst 5 mg, solvent 3 mL, reaction filled with oxygen (1 atm) every 2 h, at room temperature, white LEDs (30 × 3 W, λ ≥ 420 nm), 4 h irradiation. ^aIn the dark. ^bMechanical mixing of CdS and C₃N₄ (mass ratio, 100:30), 5 mg. ^cWithout cdcn. ^dFilled with N₂. ^eIn air. ^f5 h irradiation. ^gMethyl o-methoxyphenyl sulfide (1 mmol) as substrate, 5 h irradiation. ^hMethyl m-methoxyphenyl sulfide (1 mmol) as substrate, 5 h irradiation. Conversion and selectivity was determined by ¹H NMR.

because it is the strongest organic protic solvent and is redox active.²⁷ When CH₃OH was replaced with inert organic solvents, only slight conversion of sulfide was obtained. It has been reported that Pt/BiVO₄ systems exhibit excellent performance for the oxidation of sulfides in water compared with in organic solvents.³⁴ However, in the present catalytic system, low conversion was observed when water was used as the solvent, which might be because of the poor solubility of sulfides in water (the amount of sulfides we used is large). The experimental results of control experiments (Table 1, entries 7–12), showed that no reaction took place in the absence of photocatalyst, light, or dioxygen. The catalytic activity of mechanically mixed CdS and C₃N₄ was higher than that of bare CdS or C₃N₄, but incomparable with that of cdcn(30). This reaction conducted in air resulted in a relatively low conversion efficiency compared with that when the system was filled with dioxygen (1 atm; Table 1, entry 13). When methyl p-methoxyphenyl sulfide was replaced with methyl o-methoxyphenyl sulfide, the conversion suddenly dropped to 52.6%. Moreover, a conversion of only 11.5% was achieved when methyl m-methoxyphenyl sulfide was used as the substrate. These results strongly suggest that electronic and steric hindrance effects of the substituents in the aryl sulfides played an important role in the catalytic reaction using cdcn. As known, electron-donating groups (ED) are easier to donate electrons than electron-withdrawing groups (EW). This may be the reason for the low conversion of m-methoxyphenyl sulfide. Additionally, the steric hindrance of methyl o-methoxyphenyl sulfide led to a decrease in conversion.³⁴ Furthermore, the

conversion efficiencies obtained for substrate molecules with different groups clearly demonstrated the more important role of the electronic donor or acceptor group in the photocatalytic oxidation reaction (Table 2). Based on the above analysis and previous reports,^{27,28} it can be concluded that the presence of electron-donating groups accelerated the conversion of sulfide into sulfoxide, whereas a large steric hindrance effect was unfavorable to the photocatalytic oxidation.

Table 2 Photocatalytic oxidation of sulfides with different substitutes.

Entry	Substrate	Product	Time (h)	Conv. (%)	Sel. (%)
1			6	85.8	99
2			6	73.6	99
3			6	61.8	99
4			6	6.5	100
5			6	5.6	100

Reaction conditions: substrate 0.3 mmol, cdcn(30) 5 mg, methanol 3 mL, O₂ 1 atm, at room temperature.

¹H NMR spectra of the substrate and product in the photocatalytic oxidation reaction measured at different reaction time are shown in Fig. 5a, in which changes in the peaks were observed with increasing reaction time to 5 h. However, no difference in selectivity was observed even when the photocatalytic system was irradiated for 20 h, implying a good product selectivity. Additionally, cdcn(30) exhibited high photocatalytic activity for sulfide oxygenation compared with those of previously reported photocatalysts (Table S1) in terms of per unit mass. The reaction kinetics (Fig. 5b) for the photocatalytic oxidation of methyl p-methoxyphenyl sulfide under visible-light irradiation was also investigated in air while attempting to maintain the concentration of dioxygen. Methyl p-methoxyphenyl sulfide was almost linearly oxidized, maintaining a high selectivity towards sulfoxide. Thus, the conversion of sulfide almost followed zero-order reaction kinetics. As a heterogeneous catalyst, cdcn could be separated from the reaction solution easily by simple filtration or centrifugation. Therefore, the photostability of the hybrid catalyst, which is an important factor for practical application, could be evaluated using recycling tests (Fig. 5c). After four successive cycles, the catalyst retained its high photocatalytic activity. The XRD pattern (Fig. S6) of the used catalyst showed no significant differences with that of the as-prepared catalyst, suggesting that the crystal structures of the composite were not altered during the photocatalytic reaction. In addition, we measured the concentration of Cd²⁺ by method of linear sweep voltammetry with a bismuth film electrode (Fig. S7). The obtained results showed that the concentration of cadmium ion changed from 1.8 mg/L to 38.3 mg/L after 5 h irradiation (Fig. S8), implying the composited catalyst is stable.

3.3 Proposed mechanism

To acquire more insight into the reaction mechanism, an ESR

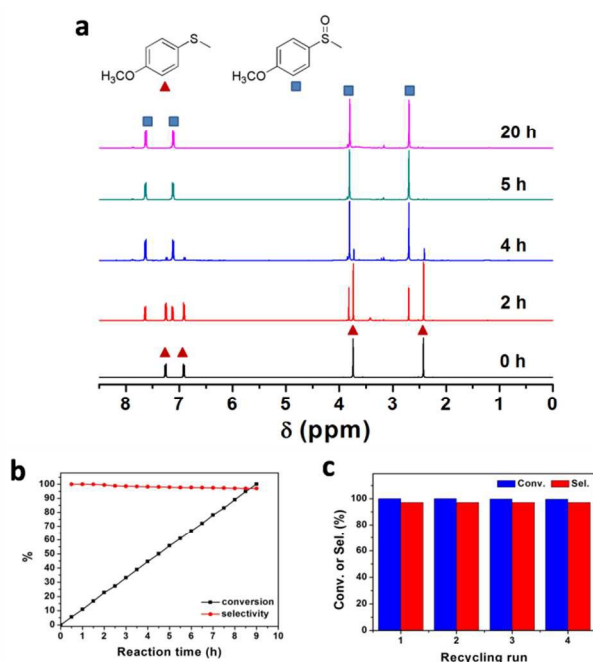


Fig. 5 (a) ¹H NMR (DMSO-d₆) spectra of methyl p-methoxyphenyl sulfide after different irradiation time. (b) Reaction kinetics plot for photocatalytic oxidation of methyl p-methoxyphenyl sulfide under visible-light irradiation in air. (c) Results of cycling test of cdcn(30). Reaction conditions: methyl p-methoxyphenyl sulfide 1 mmol, cdcn(30) 5 mg, CH₃OH 3 mL, 1 atm O₂, at room temperature.

spin-trapping technique with 5,5'-dimethyl-1-pyrroline N-oxide (DMPO) was employed to probe the reactive oxygen species generated during visible-light irradiation. The four characteristic peaks of the DMPO-O₂^{•-} adduct (Fig. 6a, b) were observed. Furthermore, this species was thermodynamically stable for the transfer of photogenerated electrons to the adsorbed O₂ to produce superoxide radicals (•O₂⁻). After adding sulfide to the system, the signals of the DMPO-O₂^{•-} adduct were remarkably weakened (Fig. 6c, d), which implies that the superoxide radical played an important role in oxygenation of sulfide in this catalytic system. Notably, hydroxyl radicals were not detected in the ESR analysis. Methanol solvent can serve as a quencher of hydroxyl radicals. A series of active species trapping experiments (Table 3) were further performed to investigate the photocatalytic oxidation mechanism. It is very interesting that the reaction did not proceed when hydroquinone, a free radical scavenger, was added to the sulfide oxygenation system, which indicated that the reaction involved a free radical chain pathway. When p-benzoquinone was added to quench the superoxide radical, the conversion surprisingly dropped to 3.7%, revealing that the generated superoxide radicals were the major oxidative species involved in the selective oxidation of sulfide to sulfoxide. Besides the superoxide radicals, valence band holes also had an effect on sulfide oxygenation to some extent. While the quenching of electrons with tetrachloromethane had almost no influence on the conversion. These active species trapping results demonstrated that molecular oxygen trapped photogenerated electrons to produce superoxide radicals, preventing the recombination of the photogenerated charge carriers.

On the basis of the above results, a possible mechanism for the photocatalytic oxidation of sulfide on cdcn is illustrated in

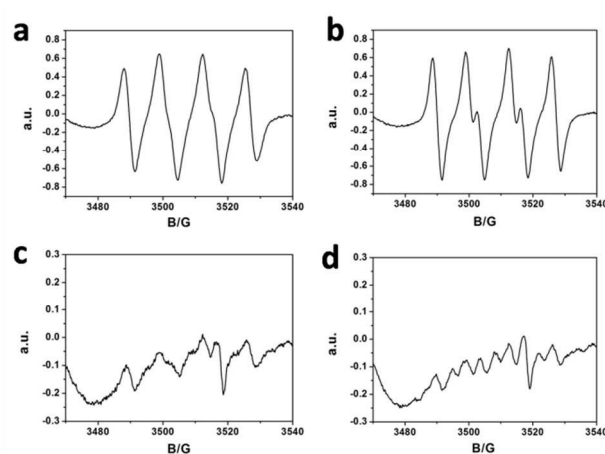


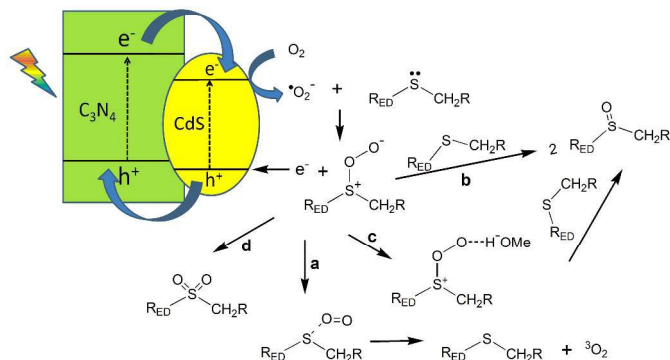
Fig. 6 Changes in ESR spectra for a system containing DMPO, cdcn(30) (2 mg) in methanol under visible-light irradiation in air. (a) Without substrate, light irradiation for 2 min, (b) for 4 min, (c) with methyl p-methoxyphenyl sulfide for 2 min, and (d) with methyl p-methoxyphenyl sulfide for 4 min.

Table 3 Results obtained after adding different quenchers to the photocatalyzed sulfide oxidation system.

Entry	Quencher	Quenching group	Conv. (%)	Sel. (%)	
				1a	1b
1	hydroquinone	free radicals	0	—	—
2	p-benzoquinone	•O ₂ ⁻	3.7	100	0
3	HCOONH ₄	hole	21.5	97	3
4	tertiary butanol	•OH	54.5	98	2
5	CCl ₄	e ⁻	88.7	98	2

Reaction conditions: methyl p-methoxyphenyl sulfide 1 mmol, cdcn(30) 5 mg, methanol 3 mL, O₂ 1 atm, visible-light irradiation for 4 h, at room temperature.

Scheme 1. Under visible-light irradiation, electrons are excited from the valence band of CdS and C₃N₄ to the conduction band, leaving holes in the valence band. The electrons on the conduction band would be trapped by electrophilic O₂ to form superoxide radicals, which is the major active species that induces sulfide oxygenation. Sulfides with electron-donating groups easily deliver electrons to the holes of the photocatalyst compared with those containing electron-withdrawing groups. Furthermore, the stability of the persulfoxide can be dramatically influenced by nearby groups of the sulfide, which with electron-donating groups can contribute electron density to the persulfoxide sulfur. It has been reported that collinear donor-persulfoxide sulfur-oxygen is beneficial for sulfide oxygenation.⁵⁰ Conversion is therefore the highest when electron-donating groups are located at the para-position. The superoxide radical can attack the sulfur atom, forming persulfoxide, which is recognized to be the key active intermediate in the whole oxidation process and is confirmed by computational and experimental evidence.^{51–53} The persulfoxide can in fact undergo either an unproductive intersystem crossing (path a) or product formation (path b). Additionally, the process of product formation in protic



Scheme 1 Possible reaction mechanism for photocatalytic sulfide oxygenation.

solvents involves an interaction between persulfoxide and solvent molecules, resulting in a second intermediate (path c).⁵¹ In addition, we conducted a set of experiments by adding acetic acid into acetonitrile, and the conversion changed from 17.0 % to 36.4 % (Table S2), supporting that protonation of weakly basic persulfoxide is the intermediate. In general, the conversion of substrate molecules with electron-withdrawing substituents is lower owing to the decreased electron density around the sulfur atom. However, path c is more efficient than path b. This is attributed to hydrogen-bonded persulfoxide, which is a stronger electrophile and thus facilitates oxygen transfer to a second sulfide molecule. The presence of substituents in the ortho-position in the chain makes the reaction less effective because the steric hindrance encountered by the approaching sulfides, which makes oxygen transfer less competitive leading to the decay of the persulfoxide. In this case, some effect is also exerted when the substituent is in the meta-position. Additionally, the corresponding sulfone may be generated via hydroxyl group migration to the sulfur atom. However, this migration is relatively difficult owing to the steric hindrance and electronic effects.

4. Conclusion

In summary, a cdcn composite photocatalyst was easily prepared at various constituent mass ratios and temperatures, allowing the oxidation of sulfide to be investigated in detail. The improved photocatalytic performance of the photocatalyst was attributed to a decreased recombination of the photogenerated electron-hole pairs, reduced aggregation of CdS, and enhanced stability, originating from the well-matched overlapping band structures and closely contacted heterojunction interfaces. The optimal catalyst was prepared with a mass ratio of C₃N₄ to CdS of 0.3 at a temperature of 300 °C with methanol as the solvent. Cdcn(30) displayed high photocatalytic activity for sulfide oxidation with O₂ under visible-light irradiation in terms of unit mass. Sulfides with electron-donating groups were efficiently oxidized to sulfoxides with high selectivity. A possible mechanism for this catalytic system was also proposed. The obtained results showed that superoxide radicals played an important role in the sulfide oxygenation, reacting with the sulfide to form an active persulfoxide intermediate. Protic solvents such as methanol could stabilize the persulfoxide through hydrogen bond interactions, which facilitate its electrophilic attack towards another substrate molecule. This work is expected to provide

new insights for the design of high-performance catalysts for the oxidation of sulfides.

Acknowledgements

This work was financially supported by the National Key Basic Research Program of China (973 Program 2013CB834804), the Ministry of Science and Technology (2012DFH40090). We thank the National Natural Science Foundation of China (21273257, 21267025, 21471155 and U1137606) for financial support.

Notes and references

^aKey Laboratory of Photochemical Conversion and Optoelectronic Materials and HKU-CAS Joint Laboratory on New Materials, Technical Institute of Physics and Chemistry, University of Chinese Academy of Sciences, Chinese Academy of Sciences, Beijing 100190, P.R. China

E-mail: fuw@ipc.ac.cn

^bCollege of Chemistry and Chemical Engineering, Yunnan Normal University, Kunming 650092, P.R. China

†Electronic Supplementary Information (ESI) available. See DOI:10.1039/b000000x/

- Q. Y. Meng, J. J. Zhong, Q. Liu, X. W. Gao, H. H. Zhang, T. Lei, Z. J. Li, K. Feng, B. Chen, C. H. Tung and L. Z. Wu, *J. Am. Chem. Soc.*, 2013, **135**, 19052–19055.
- J. Xuan, X. D. Xia, T. T. Zeng, Z. J. Feng, J. R. Chen, L. Q. Lu and W. J. Xiao, *Angew. Chem. Int. Ed.*, 2014, **53**, 5653–5656.
- A. H. Ye, W. Q. Fan, Q. H. Zhang, W. P. Deng and Y. Wang, *Catal. Sci. Technol.*, 2012, **2**, 969–978.
- N. Zhang, Y. H. Zhang, X. Y. Pan, X. Z. Fu, S. Q. Liu and Y. J. Xu, *J. Phys. Chem. C*, 2011, **115**, 23501–23511.
- Y. H. Zhang, N. Zhang, Z. R. Tang and Y. J. Xu, *Chem. Sci.*, 2012, **3**, 2812–2822.
- K. Bahrami, *Tetrahedron Lett.*, 2006, **47**, 2009–2012.
- K. Kaczorowska, Z. Kolarska, K. Mitka and P. Kowalski, *Tetrahedron*, 2005, **61**, 8315–8327.
- C. G. Venier, T. G. Squires, Y. Y. Chen, G. P. Hussmann, J. C. Shei and B. F. Smith, *J. Org. Chem.*, 1982, **47**, 3774–3777.
- S. Wolfe and C. F. Ingold, *J. Am. Chem. Soc.*, 1983, **105**, 7755–7757.
- F. Gasparri, M. Giovannoli, L. Maresca, G. Natile and G. Palmieri, *Synth. Commun.*, 1984, **14**, 1111–1117.
- A. Foroumadi, M. Daneshalab, M. Mahmoudian, M. Falahati, N. Nateghian, N. Shahsavarani and A. Shafiee, *Pharm. Pharmacol. Commun.*, 1998, **4**, 95–98.
- L. Xu, J. Cheng and M. L. Trudell, *J. Org. Chem.*, 2003, **68**, 5388–5391.
- P. S. Nico and R. J. Zasoski, *Environ. Sci. Technol.*, 2001, **35**, 3338–3343.
- N. Xie, R. A. Binstead, E. Block, W. D. Chandler, D. G. Lee, T. J. Meyer and M. Thiruvazhi, *J. Org. Chem.*, 2000, **65**, 1008–1015.
- X. R. Zhou, X. Chen, Y. Q. Jin and I. E. MarkÓ, *Chem. Asian J.*, 2012, **7**, 2253–2257.
- H. Egami and T. Katsuki, *J. Am. Chem. Soc.*, 2007, **129**, 8940–8941.
- S. E. Martín and L. I. Rossi, *Tetrahedron Lett.*, 2001, **42**, 7147–7151.

ARTICLE

18. K. Jeyakumar and D. K. Chand, *Tetrahedron Lett.*, 2006, **47**, 4573–4576.
19. J. K. Li, X. Q. Huang, S. Yang, Y. Q. Xu and C. W. Hu, *Cryst. Growth. Des.*, 2015, **15**, 1907–1914.
20. V. M. Dembitsky, *Tetrahedron*, 2003, **59**, 4701–4720.
21. P. Guillo, O. Hamelin, P. Bataat, G. Jonusauskas, N. D. McClenaghan and S. Ménage, *Inorg. Chem.*, 2012, **51**, 2222–2230.
22. O. Hamelin, P. Guillo, F. Loiseau, M. F. Boissonnet and S. Ménage, *Inorg. Chem.*, 2011, **50**, 7952–7954.
23. T. T. Li, F. M. Li, W. L. Zhao, Y. H. Tian, Y. Chen, R. Cai and W. F. Fu, *Inorg. Chem.*, 2015, **54**, 183–191.
24. X. Zhou, F. Li, X. N. Li, H. Li, Y. Wang and L. C. Sun, *Dalton Trans.*, 2015, **44**, 475–479.
25. A. Company, G. Sabenya, M. González-Béjar, L. Gómez, M. Clémancey, G. Blondin, A. J. Jasniewski, M. Puri, W. R. Browne, J. M. Latour, L. Q. Jr, M. Costas, J. Pérez-Prieto and J. Lloret-Fillol, *J. Am. Chem. Soc.*, 2014, **136**, 4624–4633.
26. Q. Wang, M. Zhang, C. C. Chen, W. H. Ma and J. C. Zhao, *Angew. Chem. Int. Ed.*, 2010, **49**, 7976–7979.
27. X. J. Lang, W. R. Leow, J. C. Zhao and X. D. Chen, *Chem. Sci.*, 2015, **6**, 1075–1082.
28. X. J. Lang, W. Hao, W. R. Leow, S. Z. Li, J. C. Zhao and X. D. Chen, *Chem. Sci.*, 2015, **6**, 5000–5005.
29. P. F. Zhang, Y. Wang, H. R. Li and M. Antonietti, *Green Chem.*, 2012, **14**, 1904–1908.
30. N. Zhang, M. Q. Yang, S. Q. Liu, Y. G. Sun and Y. J. Xu, *Chem. Rev.*, 2015, **115**, 10307–10377.
31. F. Z. Su, S. C. Mathew, G. Lipner, X. Z. Fu, M. Antonietti, S. Blechert and X. C. Wang, *J. Am. Chem. Soc.*, 2010, **132**, 16299–16301.
32. F. Z. Su, M. Antonietti and X. C. Wang, *Catal. Sci. Technol.*, 2012, **2**, 1005–1009.
33. X. H. Li, J. S. Chen, X. C. Wang, J. H. Sun and M. Antonietti, *J. Am. Chem. Soc.*, 2011, **133**, 8074–8077.
34. B. Zhang, J. Li, B. Q. Zhang, R. F. Chong, R. G. Li, B. Yuan, S. M. Lu, C. Li, *J. Catal.*, 2015, **332**, 95–100.
35. S. Cao, Y. Chen, C. J. Wang, P. He and W. F. Fu, *Chem. Commun.*, 2014, **50**, 10427–10429.
36. Y. X. Pan, T. H. Zhou, J. Y. Han, J. D. Hong, Y. B. Wang, W. Zhang and R. Xu, *Catal. Sci. Technol.*, 2016, **6**, 2206–2213.
37. S. Q. Liu, M. Q. Yang, Z. R. Tang and Y. J. Xu, *Nanoscale*, 2014, **6**, 7193–7198.
38. M. Q. Yang and Y. J. Xu, *Phys. Chem. Chem. Phys.*, 2013, **15**, 19102–19118.
39. J. Y. Zhang, Y. H. Wang, J. Jin, J. Zhang, Z. Lin, F. Huang and J. G. Yu, *ACS Appl. Mater. Interfaces*, 2013, **5**, 10317–10324.
40. J. H. Liu, Y. W. Zhang, L. H. Lu, G. Wu and W. Chen, *Chem. Commun.*, 2012, **48**, 8826–8828.
41. H. J. Yan, J. H. Yang, G. J. Ma, G. P. Wu, X. Zong, Z. B. Lei, J. Y. Shi, *J. Catal.*, 2009, **266**, 165–168.
42. D. J. Martin, P. J. T. Reardon, S. J. A. Moniz and J. W. Tang, *J. Am. Chem. Soc.*, 2014, **136**, 12568–12571.
43. L. Q. Ye, J. Y. Liu, Z. Jiang, T. Y. Peng, L. Zan, *Appl. Catal. B: Environ.*, 2013, **142**, 1–7.
44. Y. Wang, X. C. Wang and M. Antonietti, *Angew. Chem. Int. Ed.*, 2012, **51**, 68–89.
45. Q. J. Xiang, Y. J. Guo and M. Jaroniec, *J. Phys. Chem. C*, 2011, **115**, 7355–7363.
46. F. X. Xiao, J. W. Miao and B. Liu, *J. Am. Chem. Soc.*, 2014, **136**, 1559–1569.
47. M. A. Butler, *J. Appl. Phys.*, 1977, **48**, 1914–1920.
48. S. X. Weng, B. B. Chen, L. Y. Xie, Z. Y. Zheng and P. Liu, *J. Mater. Chem. A*, 2013, **1**, 3068–3075.
49. Y. X. Yu, W. X. Ouyang, Z. T. Liao, B. B. Du and W. D. Zhang, *ACS Appl. Mater. Interfaces*, 2014, **6**, 8467–8474.
50. E. L. Clennan and S. E. Hightower, *Heteroatom Chem.*, 2007, **18**, 591–599.
51. S. M. Bonesi, M. Fagnoni and A. Albini, *J. Org. Chem.*, 2004, **69**, 928–935.
52. F. Jensen, A. Greer and E. L. Clennan, *J. Am. Chem. Soc.*, 1998, **120**, 4439–4449.
53. M. L. McKee, *J. Am. Chem. Soc.*, 1998, **120**, 3963–3969.

Journal Name

Graphical abstract:

CdS/C₃N₄ visible-light catalyst exhibits high product selectivity towards photocatalytic oxidation of sulfides into corresponding sulfoxides with dioxygen in methanol.

